Journal of Materials Chemistry C

PAPER

View Article Online
View Journal | View Issue

Cite this: J. Mater. Chem. C, 2015, 3, 5285

An *in situ* SERS study of substrate-dependent surface plasmon induced aromatic nitration†

Wei Huang,‡[a] Qiang Jing,‡[a] Yunchen Du,*[a] Bin Zhang,[a] Xiangli Meng,[a] Mengtao Sun,[b] Kirk S. Schanze,[c] Hong Gao[d] and Ping Xu*[a]

Received 27th March 2015,
Accepted 20th April 2015

DOI: 10.1039/c5tc00835b

www.rsc.org/MaterialsC

Here we demonstrate the surface plasmon (SP) induced nitration of aromatic rings by an *in situ* surface enhanced Raman spectroscopy (SERS) technique. The size feature of the as-prepared Au, Ag and Ag@PDA@Au hierarchical structures allows monitoring the entire reaction process on a single hierarchical structure. With benzenethiol (BT) and HNO_3 as reactants, SP induced aromatic nitration can be successfully realized without the assistance of a conventional acid catalyst, H_2SO_4. Experimental and theoretical studies confirm that the nitration reaction leads to *para*-nitrothiophenol (*p*-NTP). While control experiments show that SP here functions as a local heating source and the presence of metal is also necessary for this nitration reaction. This SP induced aromatic nitration reaction also displays SERS substrate-dependent reaction kinetics, which proceeds more rapidly on the Au surface. Higher laser power can generate a stronger photothermal effect, and thus an accelerated reaction rate for this reaction. We believe this finding may broaden the research areas in the SP assisted or induced catalytic reactions.

Introduction

Surface plasmon resonance (SPR) can be described as the resonant photon-induced collective oscillation of valence electrons, generated when the frequency of photons matches the natural frequency of surface electrons oscillating against the restoring force of positive nuclei.[1–3] SPR is characterized by a build-up of intense, spatially non-homogeneous oscillating electric fields in the neighborhood or at the surface of the nanostructured materials. In recent years, surface plasmon (SP) has been widely applied in assisting or inducing catalytic reactions.[4] In the semiconductor–metal hybrid systems, SP produced from metal nanoparticles can dramatically enhance the photocatalytic activities in the fields of water splitting,[5–8] hydrogen generation,[9–12] and chemical energy conversion.[13–15] In these reaction processes, SP mainly plays a role in facilitating electron–hole separation for the semiconductors. Very recently, it has been demonstrated that SP itself can induce catalytic reactions, either as a hot electron source or a plasmonic heating source. Coupling (azo formation) reactions from either amine or nitro groups have been intensively studied on metal nanostructure surfaces by surface enhanced Raman spectroscopy (SERS) and tip-enhanced Raman spectroscopy (TERS) techniques.[16–27] Since then, chemical reactions that can be realized directly by SP induction have been widely reported. With SP generated on the metal surface, Suzuki coupling reactions can occur on Au–Pd nanostructures under visible light irradiation.[28] SP induced reduction of graphene oxide (GO) to reduced graphene oxide (RGO) during SERS measurements was discovered, with Ag nanoparticles decorated on the GO surface.[29] Scherman *et al.* found that a prototypical stilbene photoreaction could be monitored *in situ* by SERS, using self-assembled gold nanoparticles linked by the sub-nm macrocycle cucurbit[*n*]uril (CB[*n*]) as nanoreactors.[30] Sun *et al.* reported that molecule design (removal or decoration of functional groups) could be realized by using the so-called "plasmonic scissors".[31] More recently, Fe^{3+} to Fe^{2+} reduction by plasmonically generated hot electrons from Ag nanoparticles has also been evidenced by SERS.[32] Halas *et al.* observed plasmon-induced dissociation of H_2 and doping of graphene by hot electrons generated from Au nanoparticles.[33,34] It can be seen that SP induced catalysis is an on-going research area, which might open up new avenues in the investigation of novel catalytic techniques.

Although coupling (azo formation) reactions from either amine or nitro groups have been witnessed by direct SP assistance, the discovery of other catalytic reactions that can be induced by SP and *in situ* monitored by the SERS technique has been in a very slow process. Herein, we demonstrate the SERS substrate-dependent SP induced catalytic aromatic nitration by an *in situ* single particle SERS technique. *p*-Nitrothiophenol (*p*-NTP) can be synthesized

[a] Department of Chemistry, Harbin Institute of Technology, Harbin 150001, China. E-mail: pxu@hit.edu.cn, yunchendu@hit.edu.cn
[b] Institute of Physics, Chinese Academy of Sciences, Beijing 100090, China
[c] Department of Chemistry, University of Florida, Gainesville, FL 32611, USA
[d] Key Laboratory for Photonic and Electric Bandgap Materials, Ministry of Education, Harbin Normal University, Harbin 150025, China

† Electronic supplementary information (ESI) available: Fig. S1–S14. See DOI: 10.1039/c5tc00835b

‡ These two authors contributed equally to this work.

from benzenethiol (BT) and nitric acid (HNO_3) by continuous laser excitation, without the presence of a conventional acid catalyst, H_2SO_4, and the reaction kinetics are dependent on the nature of SERS substrates. We believe this plasmon-driven nitration reaction will open up new avenues in the field of surface plasmon induced or assisted catalysis.

Experimental section

Preparation of Ag particles

Hierarchical Ag particles were prepared according to a previous procedure.[35] In a typical synthesis, 1 ml of 1 M $AgNO_3$ aqueous solution and 50 μL of 0.1 M citric acid were added into 10 ml of deionized water in a 25 ml beaker with a magnetic stirrer in an ice-water bath. 10 min later, ascorbic acid aqueous solution (1 M) was quickly injected into the vigorously stirred mixture. The color of the solution became gray or black along with a large number of silver particles produced in a few minutes. The reaction was terminated at a reaction time of 15 min by centrifugation, and the silver particles were collected. The obtained particles were repeatedly rinsed with deionized water and ethanol to remove the surface adsorbed molecules. Then the samples were dried in a vacuum drier to prevent the oxidation of the Ag surface.

Preparation of Ag@PDA particles

5 mg of the as-prepared Ag microspheres were dispersed in 20 ml of 0.002 g ml^{-1} dopamine aqueous solution. Dopamine would be self-polymerized into polydopamine (PDA) after adding a tris buffer solution.[36] 5 ml of 0.001 g ml^{-1} tris buffer solution was added quickly into the dopamine aqueous solution under vigorous stirring. To control the thickness of the PDA layer, the polymerization lasted for 5 min. Then the Ag@PDA particles were collected by centrifugation. The obtained particles were repeatedly rinsed with deionized water and ethanol to remove the surface adsorbed molecules. Then the samples were dried in a vacuum drier.

Preparation of Ag@PDA@Au particles

5 mg of the Ag@PDA particles were re-dispersed into 10 ml of deionized water, and then 4 ml of 5 mM $HAuCl_4$ aqueous solution was added under vigorous stirring. After a reaction time of 10 min, the particles were collected by centrifugation and washed first with ammonia solution and then with water and ethanol to obtain the Ag@PDA@Au particles. Then the samples were dried in a vacuum drier.

Preparation of Au particles

Au particles were prepared according to a previous procedure.[37] In a typical procedure, 5 ml 0.1 M L-ascorbic acid was introduced dropwise into 5 ml 20 mM tetrachloroauric acid under vigorous stirring conditions. The solution was then stirred for 30 min at room temperature. The Au particles were centrifuged and redispersed in water three times to remove the excess reactants in the solution.

In situ SERS measurements

To study the surface plasmon induced nitration reaction, Ag, Au, and Ag@PDA@Au particles were firstly soaked in a mixture solution of benzenethiol in ethanol (0.1 ml/20 ml) and diluted HNO_3 in ethanol (2%) for about 30 min. The particles were then collected by centrifugation and washed by ethanol several times to remove the surface residuals. The particles were dispersed into ethanol and then transformed onto microscope glass slide by drop casting before SERS measurements were conducted. During measurement, the laser beam was focused on a single particle. Time-dependent SERS spectra were recorded under continuous 633 nm laser excitation on a Renishaw *via* a confocal Raman system. The applied laser power can be adjusted on the Raman system.

Characterization

Powder X-ray diffraction (XRD) patterns of the samples were obtained on an XRD-6000 (Shimadzu) using a CuKα source (λ = 0.154056 nm). Transmission electron microscope (TEM, Tecnai G2 F20) and scanning electron microscope (SEM, FEI Quanta 200F) were applied to observe the particle size and surface morphology.

Theoretical calculations

The DFT calculation was conducted using GAUSSIAN 09 Revision A02 at the B3LYP level of the theory with the LanL2DZ basis set for the Au atom and 6-31G(d) basis sets for other atoms. The Au_6 cluster was used in the calculations as a model of the Au substrate. The Raman frequency was scaled by 0.9652.

Results and discussion

In our previous work, we have studied the azo formation from amine or nitro groups using a single particle SERS technique, where one single hierarchical Ag microsphere prepared through an acid-directed route was used as an independent SERS platform.[23] The advantage of this technique lies in the fact that the size feature of the Ag microsphere allows its accurate location using an optical microscope on the Raman system, and its surface nanostructure guarantees strong SP generation for molecular sensing. Here, in order to investigate the effect of the SERS substrates on the SP induced aromatic nitration reaction, different substrates were fabricated. The Ag microspheres prepared according to our acid-directed procedure are about 3 μm in size,[35] with distinct surface nanostructures (Fig. 1a). Meatball-like Au microspheres are prepared following the route of a previous literature,[37] which have an average size of about 2 μm and nanoparticles that are 50–100 nm on the surface (Fig. 1f). Another structure, consisting of Au nanoparticles decorated on the as-prepared Ag microspheres, was designed and synthesized. Au can be directly produced by a galvanic replacement process from the reaction of $HAuCl_4$ and Ag, which however will lead to structure collapse of the microspheres (see Fig. S1 in ESI†). Therefore, we designed a hierarchical structure consisting of a Ag core, a polydopamine

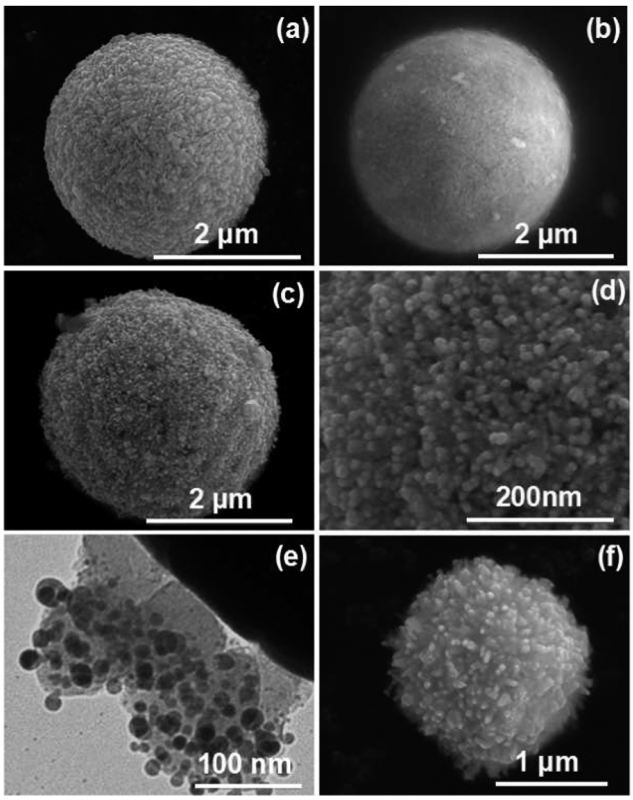

Fig. 1 SEM image of the as-prepared (a) Ag particles, (b) Ag@PDA particles, (c, d) Ag@PDA@Au particles, (f) Au particles, and magnified TEM image (e) of the Ag@PDA@Au particles showing the Au nanoparticles decorated on the PDA layer.

(PDA) protection layer, and an Au shell. The PDA protection layer was formed by soaking the Ag microspheres in a dopamine aqueous solution for 5 min, where dopamine would be self-polymerized into PDA after adding a tris buffer solution.[36] The surface nanostructure of the Ag microspheres has been modified by the formed PDA layer of the Ag@PDA particles (Fig. 1b), which makes the Ag nanostructures unable to be distinguished in detail. The Ag@PDA particles were re-dispersed into water, and an aqueous solution of $HAuCl_4$ was added. Au nanoparticles can be readily grown on the PDA layer since PDA has been demonstrated to possess a weak reducing ability.[36] Here, we found that $AuCl_4^-$ ions could still penetrate into the Ag surface through the PDA layer and react with Ag, leading to the production of AgCl cubes on the PDA surface (see Fig. S2 in ESI†), following the reaction

$$AuCl_4^- + 3Ag \rightarrow Au + 3AgCl + Cl^- \quad (1)$$

However, washing the as-obtained particles in ammonia solution effectively removes the AgCl cubes (eqn (2)), resulting in well-defined hierarchical Ag@PDA@Au microspheres with slightly increased size compared to the Ag core particles (Fig. 1c).

$$AgCl + 2NH_3{\cdot}H_2O \rightarrow [Ag(NH_3)_2]^+ + Cl^- + 2H_2O \quad (2)$$

From the magnified SEM image in Fig. 1d, one can clearly see that the Ag microsphere surface has been modified and decorated with tiny Au nanoparticles. The successful introduction of

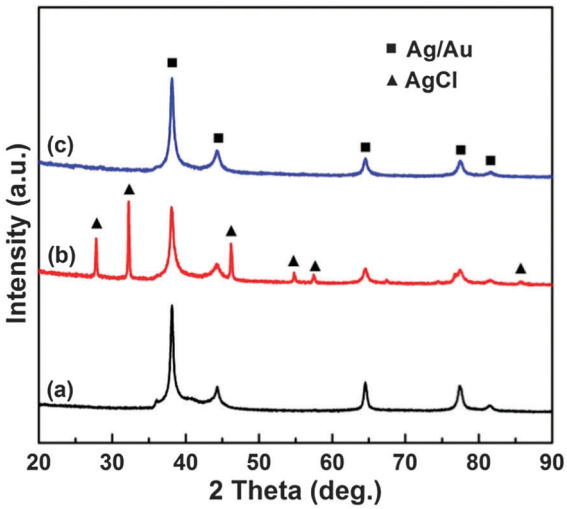

Fig. 2 XRD patterns of the as-prepared Ag particles (a), Ag@PDA after reaction with $HAuCl_4$ (b), and Ag@PDA@Au particles (c) obtained by washing sample (b) in ammonia solution.

the PDA layer and Au nanoparticles can be further verified by the TEM image in Fig. 1e. A polymer layer that is about 100 nm in thickness can be seen on the Ag surface, and the Au nanoparticles grown on the PDA surface are 10–20 nm in size. The above results indicate that the designed Ag@PDA@Au structure has been realized using our synthesis method. The uniformity of the Ag@PDA@Au hierarchical structures and their decoration with Au nanoparticles are verified by low-magnification SEM images (see Fig. S3 in ESI†).

In order to further show the reactions involved during the synthesis procedure, X-ray diffraction (XRD) patterns of the particles obtained at different stages are measured (Fig. 2). The diffraction peaks for the as-prepared Ag microspheres at 38.1, 44.3, 64.4, 77.5, and 81.5° can be indexed to the (111), (200), (220), (311), and (222) planes of the Ag crystal (PDF#04-0783). After direct reaction of Ag@PDA with $HAuCl_4$, many diffraction peaks other than those of Ag are observed. The peaks at 27.8, 32.2, 46.2, 54.8, 57.5, 67.4, and 85.7° can be ascribed to the (111), (200), (220), (311), (222), (400), and (422) planes of AgCl crystal (PDF#31-1238).[38] As mentioned above, $AuCl_4^-$ ions diffused onto the Ag surface through the PDA layer can react with Ag to produce AgCl cubes (see Fig. S2 in ESI†). However, these AgCl cubes can be eliminated by rinsing the particles in ammonia solution carefully. As can be seen, diffraction peaks assigned to Au/Ag become dominant after careful washing. The broadening of the diffraction peaks can well reflect the size and nano-scale feature at the surface of those hierarchical structures. Moreover, a comparison of the extinction spectra of the Ag, Ag@PDA, and Ag@PDA@Au particles also indicates the Au nanoparticles are successfully fabricated on the Ag@PDA surface (see Fig. S4 in ESI†). Extinction spectrum of the meatball-like Au microspheres agrees well with the previous literature (see Fig. S5 in ESI†).[37] XRD pattern of the Au particles confirms that the as-prepared sample is Au crystals in cubic phase (see Fig. S6 in ESI†).

As found, the prepared Ag microspheres and Au particles are promising SERS substrates,[35,37] while we found that the fluorescence of the PDA layer on the Ag@PDA particles makes them unsuitable in SERS studies (see Fig. S7 in ESI†). Here, Au nanoparticles that are 10–20 nm in size can generate strong surface plasmon (SP) upon light excitation, and thus the Ag@PDA@Au hierarchical structures can be readily used as SERS platforms for molecule detection. A well-resolved SERS spectrum of benzenethiol (BT) at a concentration of 10^{-8} M can be obtained on a single Ag@PDA/Au particle (see Fig. S8 in ESI†), and the peaks at 998, 1020, 1070, and 1571 cm^{-1} are due to the ν_{12}, ν_{18a}, ν_1, and ν_{8a} C–C modes of BT adsorbed on the metal surface.[39]

The nitration reaction on aromatic rings is an important industrial process, which is normally carried out in the presence of both HNO_3 and H_2SO_4. Here, we find that by focusing the laser on a single particle of the as-prepared Ag, Au or Ag@PDA@Au particles, nitration of BT occurs under continuous 633 nm laser excitation, with only BT and HNO_3 as reactants. Taking the experiments on a single Ag@PDA@Au particle for example, the nitration process can be well tracked by the time-dependent SERS spectra (Fig. 3). The peak located at 1040 cm^{-1} in the spectra arises from the ν_1 symmetric stretching of NO_3^- ions.[40,41] It can be seen that using a relatively low power of 54 μW, with the decrease in the Raman band of NO_3^- ions, a new Raman band centered at 1330 cm^{-1} was generated after an irradiation time of 10 min. After 20 min, one can hardly see the Raman band due to NO_3^-, and the intensity of the band at 1330 cm^{-1} becomes stable, indicating the completion of the reaction on a single hierarchical particle. According to a previously reported literature, the band at 1330 cm^{-1} can be assigned to the symmetric vibrational mode of the nitro group ($-NO_2$) on the benzene ring.[22] Here, it is important to understand the nitration

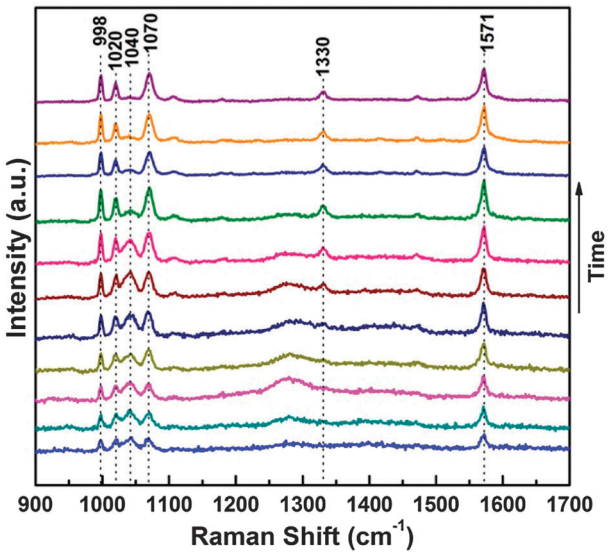

Fig. 3 Time-dependent SERS spectra showing the reaction of benzenethiol and nitric acid on a single Ag@PDA@Au hierarchical particle, with a laser wavelength of 633 nm and power of 54 μW. Spectra were recorded every 2 min under continuous laser irradiation.

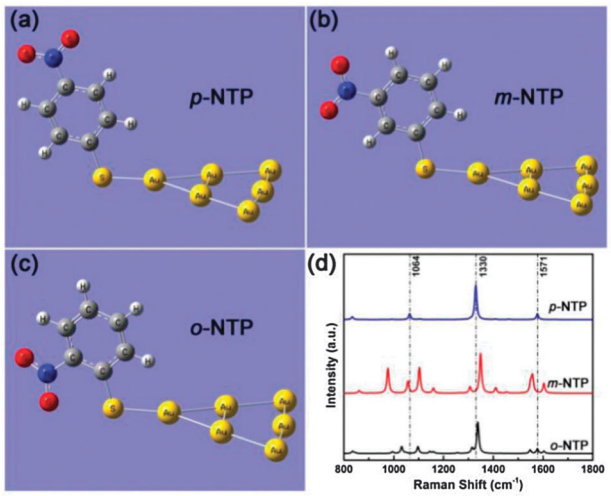

Fig. 4 Simulation models of *para*-nitrothiophenol (*p*-NTP, a), *meta*-nitrothiophenol (*m*-NTP, b), and *ortho*-nitrothiophenol (*o*-NTP, c) on Au_6 clusters from density functional theory (DFT) calculations and corresponding Raman spectra (d).

position on the benzene ring, as there are three possible products, *ortho*-nitrothiophenol (*o*-NTP), *meta*-nitrothiophenol (*m*-NTP) and *para*-nitrothiophenol (*p*-NTP). In order to clarify this, we have calculated the Raman spectra of *o*-NTP, *m*-NTP, and *p*-NTP on Au clusters based on density functional theory (DFT), as shown in Fig. 4. The symmetric vibration of the nitro group ($-NO_2$) is dominant in all three molecules, but with slight frequency shifts. Raman bands of the $-NO_2$ group for *o*-NTP, *m*-NTP, and *p*-NTP are located at 1338, 1349, and 1330 cm^{-1}, respectively, when these molecules are adsorbed onto the Au surface. Moreover, the ν_{8a} C–C mode of *p*-NTP is located at 1571 cm^{-1}, which was shifted and split into several bands for *o*-NTP and *m*-NTP. Together with the experimental results, it can be deduced that nitration of BT with HNO_3 under laser excitation prefers to occur at the *para* position on the benzene ring. This is consistent with conventional substituent positioning effect that nitration at the *para* position will be preferred when a thiol group is present on the benzene ring. More mechanistic details about the plasmon-driven catalyzed nitration reactions, based on the recently reported theoretical method,[42] are under investigation.

These results indicate that nitration on the benzene ring occurs on the Ag@PDA@Au particles upon laser irradiation. Importantly, it is found that this nitration cannot occur in the dark, as it is not possible to detect the $-NO_2$ band in the Raman spectrum when the Ag@PDA@Au particle adsorbed with BT and HNO_3 was kept in the dark under ambient conditions for more than 1 h (see Fig. S9 in ESI†). This means SP generated from Au nanoparticles induces the occurrence of this nitration reaction. Moreover, it has been found that the reaction rate is sensitive to the incident laser power. As shown in Fig. 5, at an elevated power of 0.3 mW, the Raman band corresponding to the $-NO_2$ group can be seen almost immediately when the sample is exposed to the laser irradiation. Of note is that the $-NO_2$ band is located at 1330 cm^{-1}, indicating that the product is still *p*-NTP at this higher power. However, the reaction is

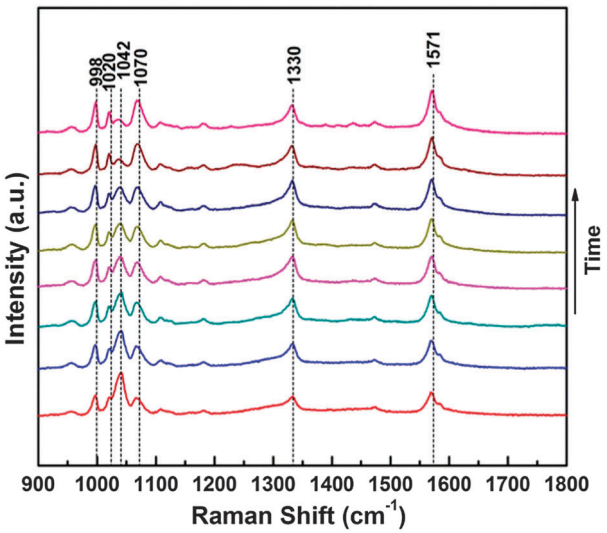

Fig. 5 Time-dependent SERS spectra showing the reaction of benzenethiol and nitric acid on a single Ag@PDA@Au hierarchical particle, with a laser wavelength of 633 nm and power of 0.3 mW. Spectra were recorded every 30 s under continuous laser irradiation.

obviously accelerated, where the Raman band of the $-NO_2$ group becomes very strong after 2 min, and is stable afterwards. This result clearly indicates that raising the laser power increases the rate of the nitration reaction. One may notice that there is a shoulder located at 1590 cm^{-1}, which is normally assigned to the $-NH_2$ group.[23] As reported, *p*-NTP can dimerize into *p*,*p*′-dimercaptoazobenzene (DMAB) through a surface plasmon mediated route,[22,24] which can further be converted into *p*-aminothiophenol (*p*-ATP) with the presence of H_2O in the environment or at the metal surface. It is also possible that *p*-NTP is directly reduced into *p*-ATP with the source of hot electrons coming from the metal upon laser excitation and the protons from HNO_3. Actually, strong acidic environment (HNO_3 involved and concentrated at the metal surface) may prohibit the reaction of converting *p*-NTP into DMAB, as it has been reported that conversion of *p*-NTP into DMAB is not possible at pH = 1.1, with HCl as a pH regulator.[17]

These data, taken together, strongly suggest that nitration of BT can occur with HNO_3 under continuous laser excitation, without the assistance of the conventional acid catalyst H_2SO_4. One may wonder how SP is involved in this nitration reaction. As we have previously noted in the SP induced dimerization of *p*-ATP, SP can function either as a hot electron source or plasmonic heating source.[23] Here, for the nitration reaction of the benzene ring (a substitution reaction), redox chemistry is not involved. If hot electrons generated from SP decay are involved, a reduction reaction should be observed. Therefore, we believe in this case, SP acts by heating the molecules adsorbed at the metal surface (Au nanoparticles) during the nitration reaction, and the local temperature can reach as high as more than 100 °C.[23] Actually, the plasmonic heating effect from metal nanoparticles upon light excitation has been verified recently in several systems.[43,44]

Two control experiments were carried out to support that plasmonic heating actually induces this nitration reaction on the metal surface. First, the nitration reaction can be clearly seen when heating a mixture of BT and HNO_3 in the presence of the Ag@PDA@Au particles at temperatures above 35 °C (see Fig. S10 in ESI†). A time-dependent study shows that this nitration reaction occurs after 5 min at 65 °C (see Fig. S11 in ESI†). Second, when a mixture of only BT and HNO_3 is heated at 65 °C for half an hour, the nitration reaction is not observed (see Fig. S12 in ESI†). These results are an indication that the nitration reaction can be realized in a photothermal process, wherein the Ag@PDA@Au particles (most probably the Au) are essential for this reaction. As mentioned previously, the presence of the thiol group on the benzene ring makes the substitution at the *para* position preferable. Therefore, nitration cannot occur in the dark under ambient conditions, with the absence of Ag@PDA@Au particles. And naturally, a higher laser power, which heats the metal surface more rapidly and efficiently, can accelerate this nitration process.

One may wonder how the substrate will influence this plasmon-induced nitration reaction, besides the applied laser power. Here, a comparison of the reaction kinetics on the as-prepared Ag, Au, and Ag@PDA@Au particles was carried out. In order to clearly distinguish the nitration process, a relatively low laser power of 54 μW was applied (633 nm laser). "Time" in Fig. 6 was defined as the moment when the Raman intensity of the $-NO_2$ group got stabilized during the reaction process. It was found out that on these three different SERS substrates, the product of the plasmon-induced nitration reaction was the same, *p*-NTP, as the newly formed peak corresponding to $-NO_2$ was all located at 1330 cm^{-1} (see Fig. S13 and S14 in ESI†). However, there is indeed substrate-dependent reaction kinetics of this plasmon induced nitration process. It can be seen that on the Au surface, the reaction stabilizes from 15 min. As mentioned above, the Raman intensity of the $-NO_2$ group remains almost unchanged after 20 min on the Ag@PDA@Au particles. On the Ag particle, the reaction gets stabilized at a time period of 30 min. Combined with the

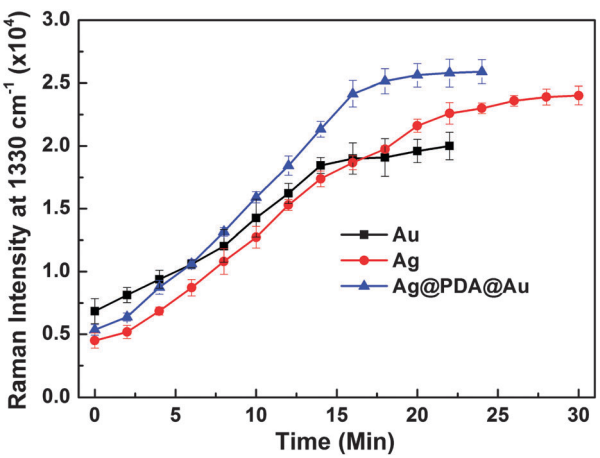

Fig. 6 Time-dependent variation of the Raman intensity corresponding to the newly formed $-NO_2$ group at 1330 cm^{-1} on different SERS substrates. Here, "time" is defined as the moment when the Raman intensity of the $-NO_2$ group became unchanged during the reaction process. The experiments were carried out with a laser wavelength of 633 nm and power of 54 μW.

control experiments, this result indicates that the metal catalyst is necessary for the plasmon induced nitration reaction, and Au surface may provide a lower energy barrier for this reaction. We have also carried out the reactions under higher laser power or other laser sources (532 nm), but the reaction follows a very rapid process, making us unable to track the detailed changes in the Raman spectra.

Conclusions

In conclusion, we have demonstrated here a study of surface plasmon (SP) induced catalytic aromatic nitration of benzenethiol by an *in situ* SERS technique on a single Ag, Au, or Ag@PDA@Au hierarchical particle. It is found that with the assistance of SP, nitration of benzenethiol molecules occurs with HNO_3 on the metal surface, in the absence of an additional catalyst such as H_2SO_4. Control experiments reveal that here SP plays a role of local heating at the metal surface, and the metal as a catalyst is also necessary for this nitration reaction. Therefore, a higher laser power applied can accelerate this nitration reaction. This SP induced aromatic nitration reaction is also SERS substrate-dependent, which proceeds faster on the Au surface. We believe this finding may open up new avenues for the study of surface plasmon assisted or induced catalytic reactions.

Acknowledgements

We thank the support from NSFC (No. 21471039, 91436102, 21203045, 11374353), Fundamental Research Funds for the Central Universities (Grant No. HIT. NSRIF. 2010065 and 2011017, PIRS of HIT A201502 and HIT. BRETIII. 201223), China Postdoctoral Science Foundation (2014M560253, 2013M541394, and 2014T70341), Postdoctoral Scientific Research Developmental Fund of Heilongjiang Province (LBH-Q14062), and Open Project Program of Key Laboratory for Photonic and Electric Bandgap Materials, Ministry of Education, Harbin Normal University, China (PEBM 201306).

Notes and references

1 H. Baida, P. Billaud, S. Marhaba, D. Christofilos, E. Cottancin, A. Crut, J. Lerme, P. Maioli, M. Pellarin, M. Broyer, N. Del Fatti, F. Vallee, A. Sanchez-Iglesias, I. Pastoriza-Santos and L. M. Liz-Marzan, *Nano Lett.*, 2009, **9**, 3463–3469.
2 O. Nicoletti, F. de la Pena, R. K. Leary, D. J. Holland, C. Ducati and P. A. Midgley, *Nature*, 2013, **502**, 80–84.
3 J. M. Luther, P. K. Jain, T. Ewers and A. P. Alivisatos, *Nat. Mater.*, 2011, **10**, 361–366.
4 P. Christopher, H. L. Xin and S. Linic, *Nat. Chem.*, 2011, **3**, 467–472.
5 Z. H. Zhang, L. B. Zhang, M. N. Hedhili, H. N. Zhang and P. Wang, *Nano Lett.*, 2013, **13**, 14–20.
6 D. B. Ingram and S. Linic, *J. Am. Chem. Soc.*, 2011, **133**, 5202–5205.
7 H. M. Chen, C. K. Chen, C. J. Chen, L. C. Cheng, P. C. Wu, B. H. Cheng, Y. Z. Ho, M. L. Tseng, Y. Y. Hsu, T. S. Chan, J. F. Lee, R. S. Liu and D. P. Tsai, *ACS Nano*, 2012, **6**, 7362–7372.
8 J. Lee, S. Mubeen, X. L. Ji, G. D. Stucky and M. Moskovits, *Nano Lett.*, 2012, **12**, 5014–5019.
9 C. G. Silva, R. Juarez, T. Marino, R. Molinari and H. Garcia, *J. Am. Chem. Soc.*, 2011, **133**, 595–602.
10 S. Mubeen, J. Lee, N. Singh, S. Kramer, G. D. Stucky and M. Moskovits, *Nat. Nanotechnol.*, 2013, **8**, 247–251.
11 M. Murdoch, G. I. N. Waterhouse, M. A. Nadeem, J. B. Metson, M. A. Keane, R. F. Howe, J. Llorca and H. Idriss, *Nat. Chem.*, 2011, **3**, 489–492.
12 Z. W. Seh, S. H. Liu, M. Low, S. Y. Zhang, Z. L. Liu, A. Mlayah and M. Y. Han, *Adv. Mater.*, 2012, **24**, 2310–2314.
13 W. B. Hou and S. B. Cronin, *Adv. Funct. Mater.*, 2013, **23**, 1612–1619.
14 S. Linic, P. Christopher and D. B. Ingram, *Nat. Mater.*, 2011, **10**, 911–921.
15 I. Thomann, B. A. Pinaud, Z. B. Chen, B. M. Clemens, T. F. Jaramillo and M. L. Brongersma, *Nano Lett.*, 2011, **11**, 3440–3446.
16 B. Dong, Y. R. Fang, X. W. Chen, H. X. Xu and M. T. Sun, *Langmuir*, 2011, **27**, 10677–10682.
17 Y. Z. Huang and B. Dong, *Sci. China: Chem.*, 2012, **55**, 2567–2572.
18 K. Kim, K. L. Kim and K. S. Shin, *Langmuir*, 2013, **29**, 183–190.
19 M. T. Sun, Y. Z. Huang, L. X. Xia, X. W. Chen and H. X. Xu, *J. Phys. Chem. C*, 2011, **115**, 9629–9636.
20 M. T. Sun and H. X. Xu, *Small*, 2012, **8**, 2777–2786.
21 M. T. Sun, Z. L. Zhang, H. R. Zheng and H. X. Xu, *Sci. Rep.*, 2012, **2**, 647.
22 L. L. Kang, P. Xu, B. Zhang, H. H. Tsai, X. J. Han and H. L. Wang, *Chem. Commun.*, 2013, **49**, 3389–3391.
23 P. Xu, L. L. Kang, N. H. Mack, K. S. Schanze, X. J. Han and H. L. Wang, *Sci. Rep.*, 2013, **3**, 2997.
24 E. M. van Schrojenstein Lantman, T. Deckert-Gaudig, A. J. G. Mank, V. Deckert and B. M. Weckhuysen, *Nat. Nanotechnol.*, 2012, **7**, 583–586.
25 L. L. Kang, P. Xu, D. T. Chen, B. Zhang, Y. C. Du, X. J. Han, Q. Li and H. L. Wang, *J. Phys. Chem. C*, 2013, **117**, 10007–10012.
26 L. B. Zhao, Y. F. Huang, D. Y. Wu and B. Ren, *Acta Chim. Sin. (Engl. Ed.)*, 2014, **72**, 1125–1138.
27 L. Kang, X. Han, J. Chu, J. Xiong, X. He, H.-L. Wang and P. Xu, *ChemCatChem*, 2015, **7**, 1004–1010.
28 F. Wang, C. H. Li, H. J. Chen, R. B. Jiang, L. D. Sun, Q. Li, J. F. Wang, J. C. Yu and C. H. Yan, *J. Am. Chem. Soc.*, 2013, **135**, 5588–5601.
29 T. S. Wu, S. Liu, Y. L. Luo, W. B. Lu, L. Wang and X. P. Sun, *Nanoscale*, 2011, **3**, 2142–2144.
30 R. W. Taylor, R. J. Coulston, F. Biedermann, S. Mahajan, J. J. Baumberg and O. A. Scherman, *Nano Lett.*, 2013, **13**, 5985–5990.
31 M. Sun, Z. Zhang, Z. H. Kim, H. Zheng and H. Xu, *Chem. – Eur. J.*, 2013, **19**, 14958–14962.

32 K. Kim, S. H. Lee, J.-Y. Choi and K. S. Shin, *J. Phys. Chem. C*, 2014, **118**, 3359–3365.
33 Z. Y. Fang, Y. M. Wang, Z. Liu, A. Schlather, P. M. Ajayan, F. H. L. Koppens, P. Nordlander and N. J. Halas, *ACS Nano*, 2012, **6**, 10222–10228.
34 S. Mukherjee, F. Libisch, N. Large, O. Neumann, L. V. Brown, J. Cheng, J. B. Lassiter, E. A. Carter, P. Nordlander and N. J. Halas, *Nano Lett.*, 2013, **13**, 240–247.
35 B. Zhang, P. Xu, X. M. Xie, H. Wei, Z. P. Li, N. H. Mack, X. J. Han, H. X. Xu and H. L. Wang, *J. Mater. Chem.*, 2011, **21**, 2495–2501.
36 H. Lee, S. M. Dellatore, W. M. Miller and P. B. Messersmith, *Science*, 2007, **318**, 426–430.
37 H. Wang and N. J. Halas, *Adv. Mater.*, 2008, **20**, 820–825.
38 Y. F. Shen, P. L. Chen, D. Xiao, C. C. Chen, M. S. Zhu, T. S. Li, W. G. Ma and M. H. Liu, *Langmuir*, 2015, **31**, 602–610.
39 M. B. Pomfret, J. J. Pietron and J. C. Owrutsky, *Langmuir*, 2010, **26**, 6809–6817.
40 G. Kang, K. Lee, H. Park, J. Lee, Y. Jung, K. Kim, B. Son and H. Park, *Talanta*, 2010, **81**, 1413–1417.
41 H. Lucas and J. P. Petitet, *J. Phys. Chem. A*, 1999, **103**, 8952–8958.
42 S. Duan, Y. J. Ai, W. Hu and Y. Luo, *J. Phys. Chem. C*, 2014, **118**, 6893–6902.
43 J. S. Donner, S. A. Thompson, C. Alonso-Ortega, J. Morales, L. G. Rico, S. I. C. O. Santos and R. Quidant, *ACS Nano*, 2013, **7**, 8666–8672.
44 J. R. Adleman, D. A. Boyd, D. G. Goodwin and D. Psaltis, *Nano Lett.*, 2009, **9**, 4417–4423.